

## 3.9 day orbital modulation in the TeV $\gamma$ -ray flux and spectrum from the X-ray binary LS 5039

F. Aharonian<sup>1</sup>, A.G. Akhperjanian<sup>2</sup>, A.R. Bazer-Bachi<sup>3</sup>, M. Beilicke<sup>4</sup>, W. Benbow<sup>1</sup>, D. Berge<sup>1</sup>, K. Bernlöhr<sup>1,5</sup>, C. Boisson<sup>6</sup>, O. Bolz<sup>1</sup>, V. Borrel<sup>3</sup>, I. Braun<sup>1</sup>, A.M. Brown<sup>7</sup>, R. Bühler<sup>1</sup>, I. Büsching<sup>8</sup>, S. Carrigan<sup>1</sup>, P.M. Chadwick<sup>7</sup>, L.-M. Chouinet<sup>9</sup>, R. Cornils<sup>4</sup>, L. Costamante<sup>1,22</sup>, B. Degrange<sup>9</sup>, H.J. Dickinson<sup>7</sup>, A. Djannati-Atai<sup>10</sup>, L.O'C. Drury<sup>11</sup>, G. Dubus<sup>9</sup>, K. Egberts<sup>1</sup>, D. Emmanoulopoulos<sup>12</sup>, P. Espigat<sup>10</sup>, F. Feinstein<sup>13</sup>, E. Ferrero<sup>12</sup>, A. Fiasson<sup>13</sup>, G. Fontaine<sup>9</sup>, Seb. Funk<sup>5</sup>, S. Funk<sup>1</sup>, M. Füßling<sup>5</sup>, Y.A. Gallant<sup>13</sup>, B. Giebels<sup>9</sup>, J.F. Glicenstein<sup>14</sup>, P. Goret<sup>14</sup>, C. Hadjichristidis<sup>7</sup>, D. Hauser<sup>1</sup>, M. Hauser<sup>12</sup>, G. Heinzelmann<sup>4</sup>, G. Henri<sup>15</sup>, G. Hermann<sup>1</sup>, J.A. Hinton<sup>1,12</sup>, A. Hoffmann<sup>16</sup>, W. Hofmann<sup>1</sup>, M. Holleran<sup>8</sup>, D. Horns<sup>16</sup>, A. Jacholkowska<sup>13</sup>, O.C. de Jager<sup>8</sup>, E. Kendziorra<sup>16</sup>, B. Khélifi<sup>9,1</sup>, Nu. Komin<sup>13</sup>, A. Konopelko<sup>5</sup>, K. Kosack<sup>1</sup>, I.J. Latham<sup>7</sup>, R. Le Gallou<sup>7</sup>, A. Lemièvre<sup>10</sup>, M. Lemoine-Goumard<sup>9</sup>, T. Lohse<sup>5</sup>, J.M. Martin<sup>6</sup>, O. Martineau-Huynh<sup>17</sup>, A. Marcowith<sup>3</sup>, C. Masterson<sup>1,22</sup>, G. Maurin<sup>10</sup>, T.J.L. McComb<sup>7</sup>, E. Moulin<sup>13</sup>, M. de Naurois<sup>17</sup>, D. Nedbal<sup>18</sup>, S.J. Nolan<sup>7</sup>, A. Noutsos<sup>7</sup>, K.J. Orford<sup>7</sup>, J.L. Osborne<sup>7</sup>, M. Ouchrif<sup>17,22</sup>, M. Panter<sup>1</sup>, G. Pelletier<sup>15</sup>, S. Pita<sup>10</sup>, G. Pühlhofer<sup>12</sup>, M. Punch<sup>10</sup>, B.C. Raubenheimer<sup>8</sup>, M. Raue<sup>4</sup>, S.M. Rayner<sup>7</sup>, A. Reimer<sup>19</sup>, O. Reimer<sup>19</sup>, J. Ripken<sup>4</sup>, L. Rob<sup>18</sup>, L. Rolland<sup>14</sup>, G. Rowell<sup>1</sup> \*, V. Sahakian<sup>2</sup>, A. Santangelo<sup>16</sup>, L. Sauge<sup>15</sup>, S. Schlenker<sup>5</sup>, R. Schlickeiser<sup>19</sup>, R. Schröder<sup>19</sup>, U. Schwanke<sup>5</sup>, S. Schwarzburg<sup>16</sup>, A. Shalchi<sup>19</sup>, H. Sol<sup>6</sup>, D. Spangler<sup>7</sup>, F. Spanier<sup>19</sup>, R. Steenkamp<sup>20</sup>, C. Stegmann<sup>21</sup>, G. Superina<sup>9</sup>, J.-P. Tavernet<sup>17</sup>, R. Terrier<sup>10</sup>, M. Tluczykont<sup>9,22</sup>, C. van Eldik<sup>1</sup>, G. Vasileiadis<sup>13</sup>, C. Venter<sup>8</sup>, P. Vincent<sup>17</sup>, H.J. Völk<sup>1</sup>, S.J. Wagner<sup>12</sup>, and M. Ward<sup>7</sup>

*Correspondence to:* denauroi@in2p3.fr, growell@physics.adelaide.edu.au

*(Affiliations can be found after the references)*

Received / Accepted

### ABSTRACT

**Aims.** New observations at very high energy (VHE)  $\gamma$ -ray energies of LS 5039, a High Mass X-ray Binary comprising a massive star and compact object, reveal that its flux and energy spectrum are modulated with the 3.9 day orbital period of the binary system. This is the first time in  $\gamma$ -ray astronomy that orbital modulation has been observed, and periodicity clearly established using ground-based  $\gamma$ -ray detectors.

**Methods.** Observations, at energies above 0.1 TeV ( $10^{11}$  eV), were carried out with the High Energy Stereoscopic System of Cherenkov Telescopes in 2005, and a time series analysis was performed on the dataset employing the Lomb-Scargle and Normalised Rayleigh statistics.

**Results.** The time series analysis reveals the existence of a highly significant (post-trial chance probability  $< 10^{-15}$ ) peak matching that of the orbital motion (determined recently via Doppler-shifted optical lines) of the compact object around the massive stellar companion. The VHE  $\gamma$ -ray emission is largely confined to half of the orbit, peaking around the inferior conjunction epoch of the compact object. For this epoch, there is also a hardening of the energy spectrum in the energy range between 0.2 TeV and a few TeV. The flux vs. orbital phase profile provides the first clear indication of  $\gamma$ -ray absorption via pair production within an astrophysical source, a process which is expected to occur if the  $\gamma$ -ray production site is situated within  $\sim 1$  AU of the compact object. Moreover the production region size must be not significantly greater than the binary separation ( $\sim 0.15$  AU). Notably, these constraints are also considerably smaller than the collimated outflows or jets (extending out to  $\sim 1000$  AU) observed in LS 5039. The spectral hardening could arise from variations with phase in the maximum electron energies, and/or the dominant VHE  $\gamma$ -ray production mechanism. This first-time observation of modulated  $\gamma$ -radiation now permits detailed studies of the complex high-energy astrophysics taking place in X-ray binary systems.

## 1. Introduction

X-ray binaries (XRBs) comprise a compact object such as a neutron star or black hole in orbit with a companion star. They are one of several types of astrophysical system that can provide a periodic environment for the acceleration of particles and subsequent production of radiation. Modulation of this radiation, linked to the orbital motion of the binary system, provides key insights into the nature and location of particle acceleration and emission processes. While such modulation is often found in XRBs up to hard X-ray energies (Lewin 1995, Wen et al. 2006), until now it has not been established in any astrophysical source at  $\gamma$ -ray energies. LS 5039 (distance  $d \sim 2.5$  kpc) is a High Mass X-ray Binary (HMXRB) comprising a massive O6.5V star in a  $\sim 3.9$  day orbit around a compact object (Casares et al. 2005). Persistent milliarcsecond radio outflows (extending to  $\sim 1000$  AU) are attributed to a mildly relativistic ( $v \sim 0.2c$ ) jet (Paredes et al. 2000, 2002), which would place LS 5039 in the *microquasar* class. Microquasars are Galactic, scaled-down versions of Active Galactic Nuclei (AGN) (Mirabel 1994), and are a sub-class of XRBs. The detection of radio and X-ray emission (Bosch-Ramon et al. 2005) and its possible association with the MeV to GeV  $\gamma$ -ray sources GRO J1823–12 (Collmar 2003) and 3EG 1824–1514 (Paredes et al. 2000) suggests the presence of multi-GeV particles. Observations in 2004 (Aharonian et al. 2005b) ( $\sim 11$  hrs) with the ground-based High Energy Stereoscopic System (HESS) established a new Very High Energy (VHE)  $\gamma$ -ray source, HESS J1826–148, within 30 arcsec of the radio position of LS 5039, revealing for the first time that LS 5039, and hence XRBs, are capable of multi-TeV ( $10^{12}$  eV) particle acceleration. Indications for variability at VHE  $\gamma$ -ray energies has recently been established (Albert et al. 2006) in a similar system (LS I +61°303). Here we report on new observations of LS 5039 at TeV  $\gamma$ -ray energies, revealing that its VHE  $\gamma$ -ray emission is modulated by the orbital motion of the compact object around its massive stellar companion.

## 2. Observations, Analysis and Results

The observations were taken with the High Energy Stereoscopic System (HESS). HESS is an array of four identical Atmospheric Cherenkov Telescopes (ACT) (Aharonian et al. 2006) located in the Southern Hemisphere (Namibia, 1800 m a.s.l), and is sensitive to  $\gamma$ -rays above 0.1 TeV. The 2004 HESS observations (Aharonian et al. 2005b) have been followed up with a deeper campaign in 2005. After data quality selection, the total dataset comprises 160 pointings representing 69.2 hours observations from both 2004 and 2005. Data were analyzed, employing two separate calibration procedures (Aharonian et al. 2004) and several background rejection and direction reconstruction methods. The results

presented here are based on the combination of a semi-analytical shower model and a parametrization based on the moment method of Hillas to yield the combined likelihood of the event being initiated by a  $\gamma$ -ray primary (deNaurois et al. 2003). As we show later, a pure Hillas-based analysis, described in (Aharonian et al. 2006), also yielded consistent results.

A total of 1960  $\gamma$ -ray events (with an excess significance above the background exceeding  $+40\sigma$ ) within  $0.1^\circ$  of the VLBA radio position of LS 5039 (Ribó et al. 2002) were found. The best-fit position (in Galactic coordinates) is  $l = 16.879^\circ$ ,  $b = -1.285^\circ$  with statistical and systematic uncertainties of  $\pm 12$  and  $\pm 20$  arcsec, respectively, which is consistent with the VLBA position within the  $1\sigma$  statistical uncertainty. The  $1\sigma$  upper limit on the intrinsic source radius was found to be 28 arcsec, or  $\sim 0.3$  pc at 2.5 kpc.

A search for periodicity, by decomposing the VHE  $\gamma$ -ray flux into its frequency components, was carried out using the Lomb-Scargle Test (Scargle 1982), (Fig. 1) and Normalised Rayleigh Statistic (NRS) (deJager 1994) (Fig. 2) which are appropriate for unevenly sampled datasets typical of those taken by HESS. An obvious peak in the Lomb-Scargle periodogram occurs at the period  $3.9078 \pm 0.0015$  days (similarly observed in the NRS test), quite consistent with the orbital period determined by Casares et al. (2005) ( $3.90603 \pm 0.00017$  days) from radial velocity measurements of the stellar companion. The error in this measurement was estimated from Monte-Carlo-simulated time series containing a sinusoid above a random background. The peak is highly significant, with a post-trial probability of less than  $10^{-15}$  that it results from a statistical fluctuation. This chance probability was estimated via Monte-Carlo simulation of random fluxes and also random resampling of fluxes (Fig. 3). In Fig. 1 (middle panel) we also show the effect of subtracting the orbital period, which removes numerous satellite peaks that are beat periods of the orbital period with the various gaps present in the HESS dataset (1-day, 28-day moon cycle, 365.25-day annual), that is, rational fractions of beat periods added to the orbital period. Fig. 1 (bottom panel) also includes results obtained on the neighbouring VHE  $\gamma$ -ray source HESS J1825–137 (Aharonian et al. 2005a), which is in the same field of view (FoV) as LS 5039 and therefore observed simultaneously. The HESS J1825–137 periodogram does not show statistically significant peaks, demonstrating that the significant peak is genuinely associated with LS 5039.

The ephemeris of Casares et al. (2005), determined from Doppler-shifted optical lines (observed in 2002 and 2003), suggests the binary makeup (Fig. 4) of LS 5039 as comprising a compact object of mass  $> 1.38 M_\odot$ , in an eccentric  $e = 0.35$  orbit around a stellar companion of mass  $\sim 20 M_\odot$  (with bolometric luminosity  $L_* \sim 10^{39}$  erg s $^{-1}$ ). The separation (center-to-center) between these two components varies between  $2.2R_*$  at periastron ( $\phi = 0.0$  with reference epoch  $T_0(\text{HJD-2400000}) = 51942.59$ ) to  $4.5R_*$  at apastron ( $\phi = 0.5$ ), for a stellar radius  $R_* = 7 \times 10^{11}$  cm. A range on the system inclination angle of  $13^\circ < i < 64^\circ$

\* Present address: School of Chemistry and Physics, University of Adelaide, 5005, Australia

is inferred from the binary mass function, the companion rotation velocity, the lack of X-ray eclipses (which assumes that the X-ray emission occurs very close to the compact object) and lack of Roche lobe overflow. The phasogram (Fig. 5 top) of integral fluxes at energies  $E > 1$  TeV vs. orbital phase ( $\phi$ ) obtained on a run-by-run basis (one data run is  $\sim 28$  minutes) clearly indicates that the bulk of the VHE  $\gamma$ -ray emission is confined to roughly half of the orbital period, covering the phase interval  $\phi \sim 0.45$  to 0.9. The VHE flux maximum appears to lag somewhat behind the apastron epoch, and aligns better with *inferior conjunction* ( $\phi = 0.716$ ) of the compact object. Inferior conjunction of the compact object occurs when it is lined up along our line-of-sight in front of the stellar companion. The VHE flux minimum occurs at a phase  $\phi \sim 0.2$ , slightly further along the orbit than *superior conjunction* ( $\phi = 0.058$ ), which is when the compact object is lined up behind the stellar companion. Note that the inclination upper limit  $i < 64^\circ$  implies that direct views of both compact object and stellar companion are always available. We define here two broad phase intervals for further study: **INFC** ( $0.45 < \phi \leq 0.9$ ) encompassing inferior conjunction, and **SUPC** ( $\phi \leq 0.45$  or  $\phi > 0.01$ ) likewise for superior conjunction. The phase error ( $\Delta\phi = (T\Delta P)/P^2 = 0.01$ ) due to uncertainties in the period measurement  $\Delta P = 0.00017$  from Casares et al. (2005), the dataset length  $T \sim 1000$  days and  $P = 3.9$  days, appears to be negligible. Nevertheless, further near-future optical line observations bracketing ours at VHE  $\gamma$ -ray observations would be desirable to check for the presence of systematic drifts in the orbital period.

The energy spectrum of the VHE  $\gamma$ -ray emission, and in particular how it might vary with orbital phase, is an important diagnostic tool. The differential photon energy spectrum (see Fig. 6) (0.2 to 10.0 TeV) for **INFC** is consistent with a hard power-law where  $\Gamma = 1.85 \pm 0.06_{\text{stat}} \pm 0.1_{\text{syst}}$  with exponential cutoff at  $E_o = 8.7 \pm 2.0$  TeV (for fitted function  $dN/dE \sim E^{-\Gamma} \exp(-E/E_o)$ ). In contrast, the spectrum for **SUPC** is consistent with a relatively steep ( $\Gamma = 2.53 \pm 0.07_{\text{stat}} \pm 0.1_{\text{syst}}$ ) pure power-law (0.2 to 10 TeV) (see Fig. 6). The spectra from these phase intervals are mutually incompatible, with the probability that the same spectral shape would fit both simultaneously being  $\sim 2 \times 10^{-6}$ . Fitting a pure power-law (which is statistically sufficient at present) to narrower phase intervals of width  $\Delta\phi = 0.1$ , and restricting the fit to energies  $E \leq 5$  TeV to reduce the effect of any cutoff, also demonstrates that a harder spectrum occurs when the flux is higher (Fig. 5 middle and bottom panels). Notably, the VHE flux at  $E \sim 0.2$  TeV appears to be quite stable over phases and the strongest modulation occurs at a few TeV. We found no evidence for long-term secular variations in VHE flux on a yearly scale independent of the orbital modulation (Fig. 7). The orbital modulation represents a VHE  $\gamma$ -ray luminosity (0.2 to 10 TeV; at 2.5 kpc) variation between  $4$  to  $10 \times 10^{33}$  erg s $^{-1}$ . Spectral fits and other numerical results are summarised in Tab. 1. Finally, in Fig. 8 we show that the spectral results obtained from a pure

Hillas-based analysis using a separate calibration procedure are consistent with results from the Semi-analytical Model+Hillas results within statistical errors.

### 3. Discussion

The basic paradigm of VHE  $\gamma$ -ray production requires the presence of particles accelerated to multi-TeV energies and a target comprising photons and/or matter of sufficient density. In microquasars, particle acceleration could take place directly inside and along the jet, out to parsec-scale distances, and also at jet termination regions due to interaction with ambient matter (Heinz & Sunyaev 2002). A non-jet scenario based on acceleration in shocks created by the interaction of a pulsar wind with the wind of the stellar companion has also been suggested (Maraschi and Treves 1981, Tavani et al. 1997, Dubus 2006). The nature of the parent particles responsible for VHE  $\gamma$ -ray emission is under theoretical discussion, with both accelerated electron (Aharonian & Atoyan 1998) and hadron (Distefano et al. 2002, Romero et al. 2003) scenarios proposed. Observationally, electrons (eg. Corbel et al. 2002, Angelini et al. 2003) and hadrons (Margon 1984) are both known to be accelerated inside jets.

The orbital modulation in LS 5039, with a peak flux around inferior conjunction, minimum flux around superior conjunction, and hardening of energy spectra, provides new information about the physical processes in microquasars. This modulation is an unambiguous sign that periodic changes in the VHE  $\gamma$ -ray absorption and/or production processes are occurring, and we discuss briefly how these could arise.

**Gamma-Ray Absorption.** VHE  $\gamma$ -rays produced close enough to the stellar companion will unavoidably suffer severe absorption via pair production ( $e^+e^-$ ) on its intense optical photon field. The cross-section for pair production is dependent on the angle  $\theta$  between the VHE  $\gamma$ -ray and optical photons, and has an energy threshold varying as  $1/(1 - \cos\theta)$ . The level of absorption therefore depends on alignment between the VHE  $\gamma$ -ray production region, the star, and the observer, leading to orbital modulation of the VHE  $\gamma$ -ray flux (Protheroe and Stanev 1997, Moskalenko 1995, Böttcher and Dermer 2005 Dubus 2006). For the orbital geometry of LS 5039, in which apastron and periastron are near the inferior and superior conjunction epochs, the absorption effect provides flux maxima at the phase of inferior conjunction, when  $\gamma$  photons are emitted towards the observer parallel to stellar photons ( $\cos\theta = 1$ ), and flux minima at superior conjunction (Dubus 2006). This picture agrees well with the observed phasogram (Fig. 5), suggesting that absorption plays an important role. The VHE  $\gamma$ -ray production region must therefore be embedded within the optical photon field of the star such that the absorption optical depth  $\tau_{\gamma\gamma}$  is large ( $\geq 1$ ), which occurs within  $\sim 1$  AU of the stellar companion. Moreover the emission region cannot be significantly larger than the orbit size (semi-major axis  $\sim 0.15$  AU), otherwise the effect would smear out over all phases. A

**Table 1.** Photon energy spectra and luminosity (0.2 to 10 TeV) of the VHE  $\gamma$ -ray emission of LS 5039 for different orbital phase intervals. The broad phase intervals **INFC** and **SUPC** encompass the inferior and superior conjunction epochs. The orbital phase  $\phi$  is calculated from the ephemeris of Casares et al. (2005). The best-fit function is indicated for each phase interval. The errors quoted are statistical with systematic errors in the 10 to 15% range.

Orbital Phase Interval	$N$ $\times 10^{-12}$ [ph cm $^{-2}$ s $^{-1}$ TeV $^{-1}$ ]	$\Gamma$	$E_o$ [TeV]	Luminosity $^{\dagger}$ [erg s $^{-1}$ ]
Fit function: $dN/dE = NE^{-\Gamma} \exp(-E/E_o)$				
<b>INFC</b> ( $0.45 < \phi \leq 0.9$ )	$2.28 \pm 0.10$	$1.85 \pm 0.06$	$8.7 \pm 2.0$	$1.1 \times 10^{34}$
<b>SUPC</b> ( $\phi \leq 0.45$ ) or $\phi > 0.9$	$0.91 \pm 0.07$	$2.53 \pm 0.07$	-	$4.2 \times 10^{33}$
All Phases (time averaged)	$1.85 \pm 0.06$	$2.06 \pm 0.05$	$13.0 \pm 4.1$	$7.8 \times 10^{33}$
Power-Law fit for energies $E \leq 5$ TeV (narrow phase intervals)				
0.0–0.1	$0.84 \pm 0.17$	$2.62 \pm 0.23$		
0.1–0.2	$0.46 \pm 0.21$	$3.08 \pm 0.47$		
0.2–0.3	$0.81 \pm 0.13$	$2.46 \pm 0.20$		
0.3–0.4	$0.78 \pm 0.18$	$2.77 \pm 0.60$		
0.4–0.5	$1.88 \pm 0.27$	$2.32 \pm 0.17$		
0.5–0.6	$2.64 \pm 0.20$	$2.04 \pm 0.10$		
0.6–0.7	$2.20 \pm 0.23$	$1.88 \pm 0.13$		
0.7–0.8	$2.44 \pm 0.20$	$1.90 \pm 0.10$		
0.8–0.9	$2.96 \pm 0.17$	$1.94 \pm 0.08$		
0.9–1.0	$1.21 \pm 0.25$	$1.84 \pm 0.25$		

$\dagger$  At 2.5 kpc distance.

additional key expectation is that the strongest absorption, and hence modulation, should occur in the energy range  $E \sim 0.2$  to 2 TeV (Dubus 2006). However, the observations show that the flux at  $\sim 0.2$  TeV appears quite stable, suggesting that additional processes must be considered to explain the spectral modulation.

**Gamma-Ray Production.** VHE  $\gamma$ -ray emission can be produced by accelerated electrons through the inverse-Compton (IC) scattering of stellar photons of the companion star, and/or from accelerated hadrons through their interaction with surrounding photons and particles. The efficiency of these processes will peak around periastron ( $\phi = 0.0$ ), reflecting the minimal separation between accelerated particles and targets, and higher target photon densities. The observed phasogram is in contrast with this behaviour. However, important influences on the energy spectrum can arise from variations of the maximum energy of accelerated electrons and dominance in the radiative processes (IC and/or synchrotron emission) by which they lose energy (known as cooling). The high temperature of the companion star means that IC  $\gamma$ -ray production proceeds primarily in the deep Klein-Nishina regime (where the IC cross-section is sharply reduced compared to the Thompson regime), and the hard VHE  $\gamma$ -ray spectrum ( $\Gamma \leq 2.5$ ) implies IC is the dominant cooling mechanism. The maximum electron energy  $E_{\max}$  is derived by equating the competing acceleration and dominant radiative loss timescales. For dominant IC cooling we have (Aharonian et al. 2006)  $E_{\max} \propto (B/w)^{3.3}$ , where  $B$  is the magnetic field and  $w$  is the target photon energy density. Since  $w \propto 1/d^2$  (for binary separation  $d$ ), and assuming  $B \propto 1/d$ ,  $E_{\max}$  will increase by a factor  $\sim 10$  from periastron to apastron, leading to a spectral hardening around the apastron phase (for LS 5039, also near

inferior conjunction). For magnetic fields expected within the binary orbit,  $B \sim 1$  G, electrons with energy above  $\epsilon \approx 6[(B/G)(d/R_*)]^{-1}$  TeV $^1$  will cool via synchrotron (X-ray) radiation in preference to IC cooling. Much stronger synchrotron losses will then produce a steepening of the VHE  $\gamma$ -ray spectrum (Moderski et al. 2005) and thus the  $d$  and  $B$  dependence of this changeover energy  $\epsilon$  could also introduce a spectral hardening at apastron. It is also feasible to consider production via accelerated hadrons. For considerably larger magnetic fields, for example at the base of the jet where  $B \sim 10^5$  G could be expected, accelerated protons interacting with stellar wind particles and/or X-ray photons associated with a possible accretion disk, provide a plausible hadronic origin via the decay of neutral pions (Aharonian et al. 2006).

**Pair Cascades.** For magnetic fields  $B < 10$  G (Aharonian et al. 2006), an extra complication arises from pair cascades initiated by absorption of first generation VHE  $\gamma$ -rays (Aharonian et al. 2006, Bednarek 2006). Cascades significantly increase the transparency of the source at  $\sim$  TeV energies, reducing absorption effects. Interestingly we do observe a VHE signal (excess significance  $6.1\sigma$ ; 79  $\gamma$ -rays) in a phase interval  $\phi = 0.0 \pm 0.05$  where VHE  $\gamma$ -rays are unlikely to escape due to absorption (Dubus 2006). A cascade, or at least an additional, possibly unmodulated, component from another process may be present.

<sup>1</sup> The electron energy at which synchrotron and IC cooling times are equal.

## 4. Conclusion

In conclusion, new observations by HESS have established orbital modulation of the VHE  $\gamma$ -ray flux and energy spectrum from the XRB LS 5039. The flux vs. orbital phase profile provides the first clear indication for  $\gamma$ -ray absorption within an astrophysical source, placing tight constraints on the location and size of the VHE  $\gamma$ -ray production region. Modulation of the energy spectrum could arise from changes in the maximum energies of electrons responsible for the radiation and/or changes in the dominant radiative mechanism. These observations provide key information about the astrophysics associated with particle acceleration processes and subsequent VHE  $\gamma$ -ray production in XRBs. In particular, we are now able to begin to explore in detail the complex relationship between  $\gamma$ -ray absorption and production processes within these binary systems.

**Acknowledgements.** The support of the Namibian authorities and of the University of Namibia in facilitating the construction and operation of HESS is gratefully acknowledged, as is the support of the German Ministry for Education and Research (BMBF), the Max Planck Society, the French Ministry for Research, the CNRS-IN2P3 and the Astroparticle Interdisciplinary Programme of the CNRS, the UK Particle Physics and Astronomy Research Council (PPARC), the IPNP of Charles University, the South African Department of Science and Technology and National Research Foundation, and the University of Namibia. We appreciate the excellent work of the technical support staff in Berlin, Durham, Hamburg, Heidelberg, Palaiseau, Paris, Saclay, and Namibia in the construction and operation of the equipment. L.C., C.M., M.O., and M.T. are also affiliated with the European Associated Laboratory for Gamma-Ray Astronomy, jointly supported by CNRS and the Max Planck Society.

## References

Aharonian F., Ayotan A., 1998 *New Astron. Rev.* 42, 579

Aharonian F., Anchordogui L., Khangulyan D., Montaruli T., 2006 *Journal Phys. in press*

Aharonian F., et al., (HESS Collaboration) 2004 *Astropart. Phys.* 22, 109

Aharonian F., Akhperjanian A.G., Bazer-Bachi A.R., et al. (HESS Collaboration) 2005a *A&A* 442, L25

Aharonian, F., Akhperjanian A.G., Aye K.-M., et al. (HESS Collaboration) 2005b *Science* 309, 746

Aharonian F., Akhperjanian A.G., Bazer-Bachi A.R., et al. (HESS Collaboration) 2006 *A&A in press*

Albert J., Aliu E., Anderhub H., et al. (MAGIC Collaboration), 2006 *Science in press* astro-ph/0605549

Angelini L., N. White, L. Ball, 2003 *ApJ.* 586, L71

Bednarek W. 2006 *MNRAS submitted* astro-ph/0601657

Bosch-Ramon V., Paredes J.M., Ribó M., et al. 2005 *ApJ.* 628, 388

Böttcher M., Dermer C.D., 2005 *ApJ.* 634, L81

Casares J., Ribó M., Ribas I., Paredes J.M., et al., 2005 *MNRAS* 364, 899

Collmar W., 2003 *Proc. 4th Agile Science Workshop*, 177 Frascati (Rome)

Corbel S., Fender R.P., Tzioumis A.K., et al. 2002 *Science* 298, 196

deJager O.C., 1994 *ApJ.* 436, 239

de Naurois M., et al., 2005 *Proc. Towards a Network of Atmospheric Cherenkov Detectors VII* (Palaiseau) p.149.

Dermer C.D., Böttcher M., 2006 *ApJ. submitted* astro-ph/0512162

Distefano C., Guetta D., Waxman E., Levinson A., 2002 *ApJ.*, 575, 378

Dubus G. 2006 *A&A* 451, 9

Dubus G. 2006 *A&A in press* astro-ph/0605287

Harmon B.A., Wilson C.A., Fishman G.J., et al. 2004 *ApJ (Supp)* 154, 585

Hartman R.C., Bertsch D.L., Bloom S.D., et al., 1999 *ApJ (Supp)* 123, 79

Heinz S., Sunyaev R., 2002 *A&A* 390, 751

Lewin, W.H.G., et al., *X-Ray Binaries* (Cambridge Astrophysics Series, Cambridge University Press 1995).

Maraschi L., Treves A., 1981 *MNRAS* 194, 1

Margon B., Ann. Rev. 1984 *A&A* 22, 507

Mirabel I.F., Rodriguez L.F., 1994 *Nature* 371, 46

Moderski R., Sikora M., Coppi P.S., Aharonian F., 2005 *MNRAS* 363, 954

Moskalenko I.V., 1995 *Spa. Sci. Rev.*, 72, 593

Paredes J.M., Bosch-Ramon V., Romero G.E., 2006 *A&A submitted* astro-ph/0509095

Paredes J.M., Martí J., Ribó M., Massi M., 2000 *Science* 288, 2340

Paredes J.M., Ribó M., Ros E., Martí J., 2002 Massi M., *A&A* 393, L99

Protheroe R.J., Stanev T., 1997 *ApJ* 322, 838

Ribó M., et al., 2002 *A&A* 384, 954

Romero G.E., Torres D.F., Kaufman Bernadó M.M., Mirabel I.F., 2003 *A&A* 410, L1

Scargle J.D., 1982 *ApJ* 263, 835

Tavani M., J. Arons 1997 *ApJ* 477, 439

Wen, L., et al., 2006 *ApJ (Supp)* 163, 372

<sup>1</sup> Max-Planck-Institut für Kernphysik, P.O. Box 103980, D 69029 Heidelberg, Germany

<sup>2</sup> Yerevan Physics Institute, 2 Alikhanian Brothers St., 375036 Yerevan, Armenia

<sup>3</sup> Centre d'Etude Spatiale des Rayonnements, CNRS/UPS, 9 av. du Colonel Roche, BP 4346, F-31029 Toulouse Cedex 4, France

<sup>4</sup> Universität Hamburg, Institut für Experimentalphysik, Luruper Chaussee 149, D 22761 Hamburg, Germany

<sup>5</sup> Institut für Physik, Humboldt-Universität zu Berlin, Newtonstr. 15, D 12489 Berlin, Germany

<sup>6</sup> LUTH, UMR 8102 du CNRS, Observatoire de Paris, Section de Meudon, F-92195 Meudon Cedex, France

<sup>7</sup> University of Durham, Department of Physics, South Road, Durham DH1 3LE, U.K.

<sup>8</sup> Unit for Space Physics, North-West University, Potchefstroom 2520, South Africa

<sup>9</sup> Laboratoire Leprince-Ringuet, IN2P3/CNRS, Ecole Polytechnique, F-91128 Palaiseau, France

<sup>10</sup> APC, 11 Place Marcelin Berthelot, F-75231 Paris Cedex 05, France UMR 7164 (CNRS, Université Paris VII, CEA, Observatoire de Paris)

<sup>11</sup> Dublin Institute for Advanced Studies, 5 Merrion Square, Dublin 2, Ireland

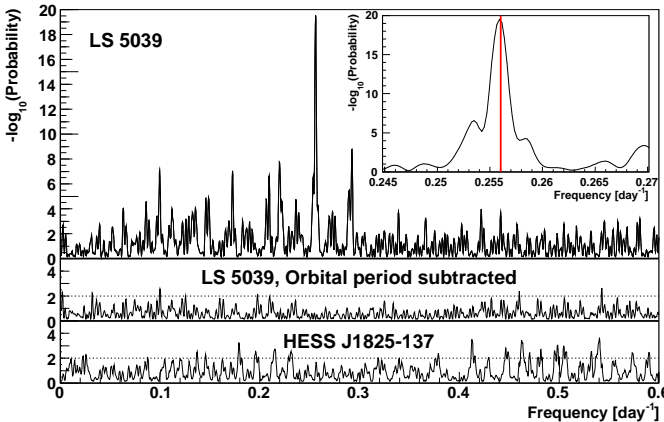


**Fig. 1. Top:** Lomb-Scargle (LS) periodogram of the VHE runwise flux for LS 5039 (chance probability to obtain the LS power vs. frequency) Inset: zoom around the highest peak (pre-trial probability  $\sim 10^{-20}$ ), which corresponds to a period of  $3.9078 \pm 0.0015$  days, compatible with the ephemeris value of  $3.90603 \pm 0.00017$  days (vertical red line at  $0.2560$  day $^{-1}$  on the inset) from Casares et al. (2005). The post-trial chance probability of the orbital period peak is found to be less than  $10^{-15}$  (see Fig. 3). **Middle:** LS periodogram of the same data after subtraction of a pure sinusoidal component at the orbital period of 3.90603 days. The orbital frequency peak has been removed as expected, as well as significant satellite peaks (see text). **Bottom:** LS periodogram of the HESS source HESS J1825–137 observed simultaneously in the same field of view. The middle and bottom panel results are consistent with that expected of white noise over the range of frequencies sampled. The dotted lines correspond to a  $10^{-2}$  pre-trial chance probability.

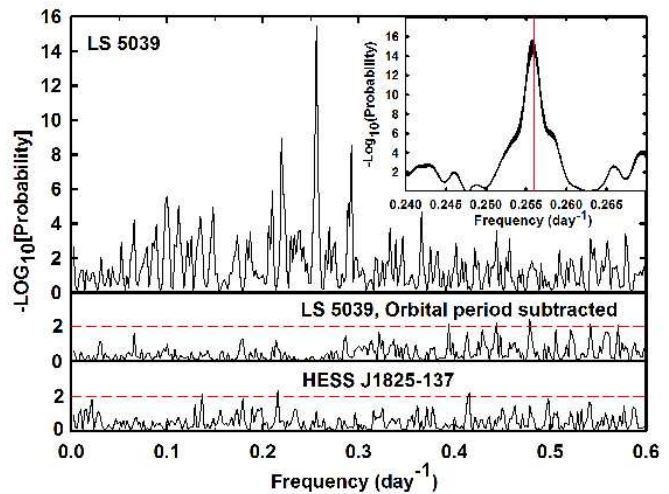


**Fig. 2. Top:** Normalised Rayleigh Statistic (deJager 1994) periodogram calculated from run-wise HESS fluxes for LS 5039. The **middle** and **bottom** panels depict the NRS after subtraction of the orbital period and for HESS J1825–137, respectively (As for the Lomb-Scargle test in Fig. 1).

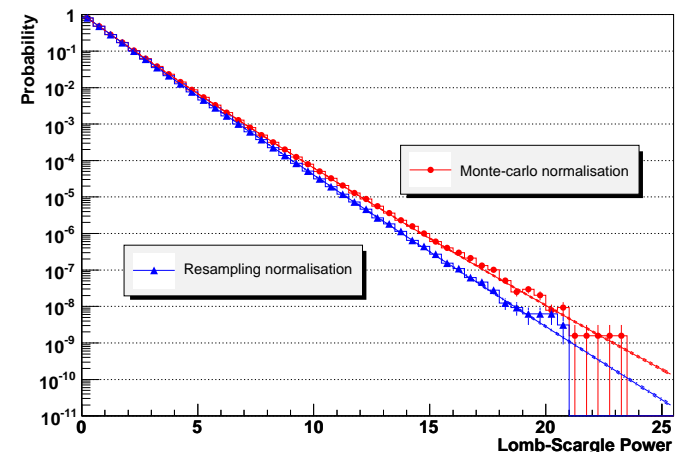


**Fig. 3.** Density function of the chance probability of the Lomb-Scargle power determined by Monte-Carlo and resampling methods after subtraction of the orbital period sinusoid. The expected exponential density functions are also indicated (solid lines). In the Monte-Carlo method,  $\sim 10^6$  random time series were generated to produce a distribution of the highest Lomb-Scargle power. The highest power obtained after these iterations reaches just above 20, well below the power of 62 obtained from the unshuffled lightcurve at the orbital period. An extrapolation of the curves is therefore used to estimate the chance probability for powers above 20.

<sup>12</sup> Landessternwarte, Universität Heidelberg, Königstuhl, D 69117 Heidelberg, Germany  
<sup>13</sup> Laboratoire de Physique Théorique et Astroparticules, IN2P3/CNRS, Université Montpellier II, CC 70, Place Eugène Bataillon, F-34095 Montpellier Cedex 5, France  
<sup>14</sup> DAPNIA/DSM/CEA, CE Saclay, F-91191 Gif-sur-Yvette, Cedex, France  
<sup>15</sup> Laboratoire d’Astrophysique de Grenoble, INSU/CNRS, Université Joseph Fourier, BP 53, F-38041 Grenoble Cedex 9, France  
<sup>16</sup> Institut für Astronomie und Astrophysik, Universität Tübingen, Sand 1, D 72076 Tübingen, Germany  
<sup>17</sup> Laboratoire de Physique Nucléaire et de Hautes Energies, IN2P3/CNRS, Universités Paris VI & VII, 4 Place Jussieu, F-75252 Paris Cedex 5, France  
<sup>18</sup> Institute of Particle and Nuclear Physics, Charles University, V Holešovickach 2, 180 00 Prague 8, Czech Republic  
<sup>19</sup> Institut für Theoretische Physik, Lehrstuhl IV: Weltraum und Astrophysik, Ruhr-Universität Bochum, D 44780 Bochum, Germany  
<sup>20</sup> University of Namibia, Private Bag 13301, Windhoek, Namibia  
<sup>21</sup> Universität Erlangen-Nürnberg, Physikalisches Institut, Erwin-Rommel-Str. 1, D 91058 Erlangen, Germany

<sup>22</sup> European Associated Laboratory for Gamma-Ray Astronomy, jointly supported by CNRS and MPG

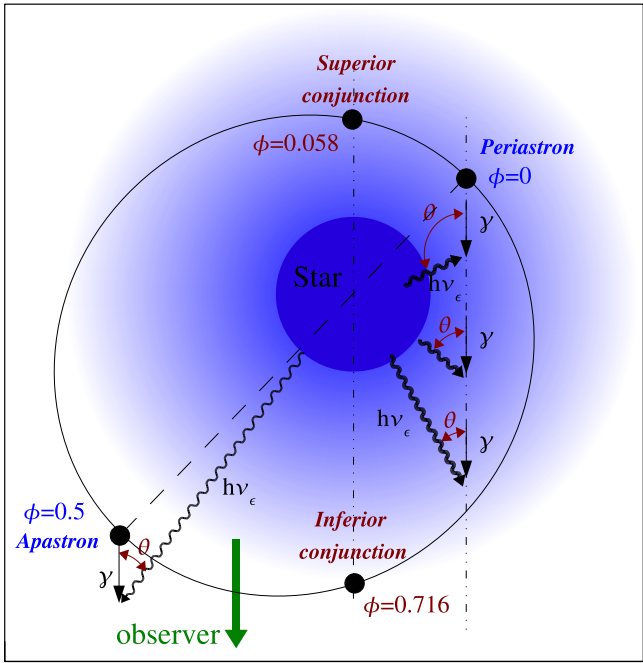


**Fig. 4.** The orbital geometry (Casares et al. 2005) viewed from directly above LS 5039. Shown are: phases ( $\phi$ ) of minimum (periastron) and maximum (apastron) separation between the two components; epochs of superior and inferior conjunctions of the compact object representing phases of co-alignment along our line-of-sight of the compact object and stellar companion. The orbit is actually inclined at an angle in the range  $13^\circ < i < 64^\circ$  with respect to the view above. VHE  $\gamma$ -rays (straight black lines with arrows) can be absorbed by optical photons of energy  $h\nu_\epsilon$ , when their scattering angle  $\theta$  exceeds zero.

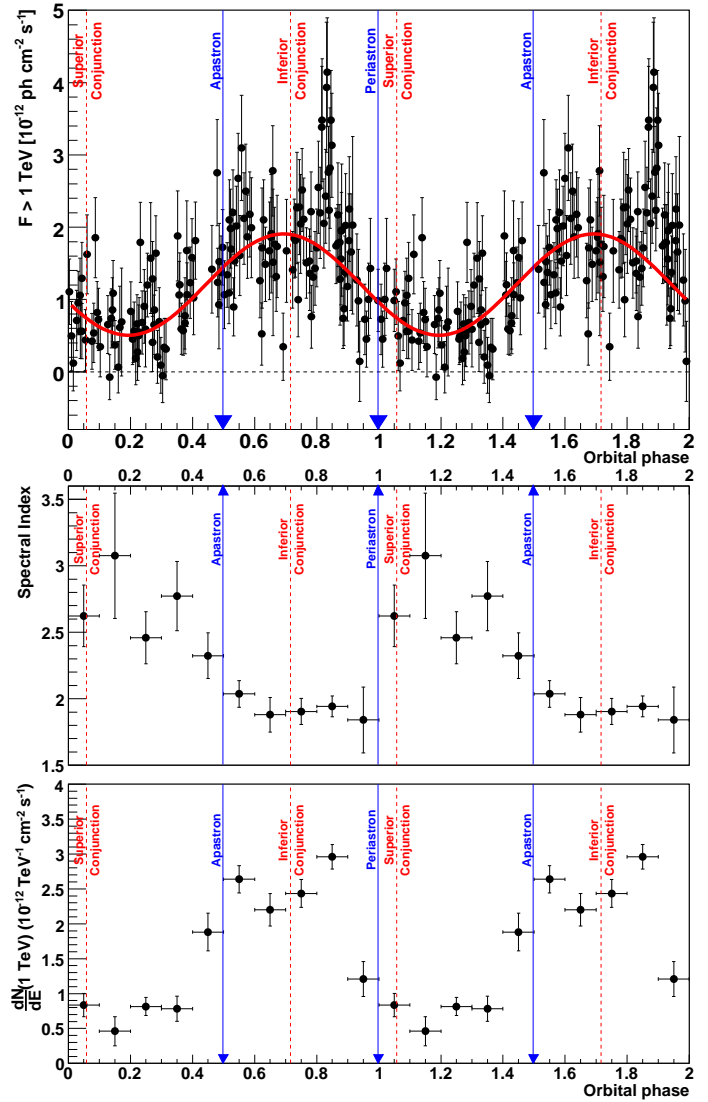


**Fig. 5. Top:** Integral  $\gamma$ -ray flux ( $F > 1$  TeV) lightcurve (phasogram) of LS 5039 from HESS data (2004 to 2005) on a run-by-run basis folded with the orbital ephemeris of Casares et al. (2005). Each run is  $\sim 28$  minutes. Two full phase ( $\phi$ ) periods are shown for clarity. The blue solid arrows depict periastron and apastron. The thin red dashed lines represent the superior and inferior conjunctions of the compact object, and the thick red dashed line depicts the Lomb-Scargle Sine coefficients for the period giving the highest Lomb-Scargle power. This coefficient is subtracted from the light curve in Fig 1 middle panel. **Middle:** Fitted pure power-law spectral index (for energies 0.2 to 5 TeV) vs. phase interval of width  $\Delta\phi = 0.1$ . Because of low statistics in each bin, more complicated functions such as a power-law with exponential cutoff provide a no better than a pure power-law. **Bottom:** Power-law normalisation (at 1 TeV) vs. phase interval of width  $\Delta\phi = 0.1$ .

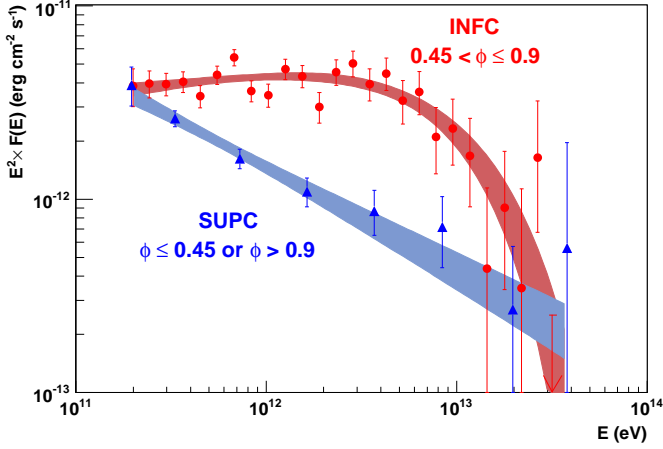


**Fig. 6.** Very high energy  $\gamma$ -ray spectra of LS 5039 for two broad orbital phase intervals (defined in the text): **INFC**  $0.45 < \phi \leq 0.9$  (red circles); **SUPC**  $\phi \leq 0.45$  or  $\phi > 0.9$  (blue triangles). The shaded regions represent the  $1\sigma$  confidence bands on the fitted functions (Tab. 1). Both spectra are mutually incompatible with the probability that the same spectral shape would fit both simultaneously being  $\sim 2 \times 10^{-6}$ . A clear spectral hardening in the region  $0.3$  to  $\sim 20$  TeV is noticed for the **INFC** phase interval.

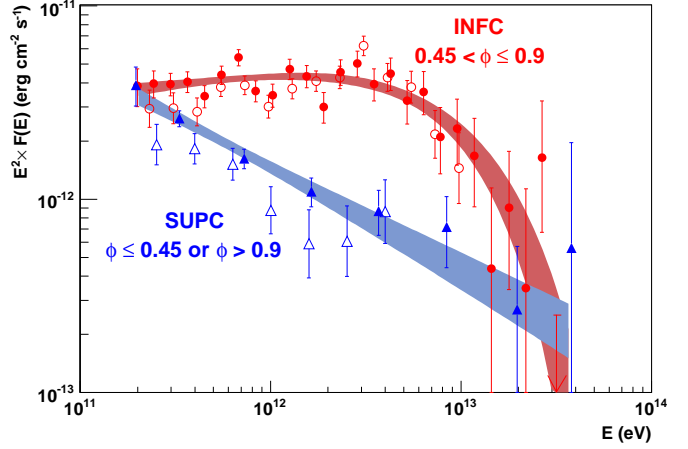


**Fig. 8.** Energy spectra of LS 5039 separated into the same broad phase intervals as for Fig. 6. **INFC**  $0.45 < \phi \leq 0.9$  (red circles); **SUPC**  $\phi \leq 0.45$  or  $\phi > 0.9$  (blue triangles), comparing results from the semi-analytical Model+Hillas (filled markers) and Hillas-only (open markers) analyses (Aharonian et al. 2006), respectively. The Hillas-only analysis has made use of an independent calibration chain.

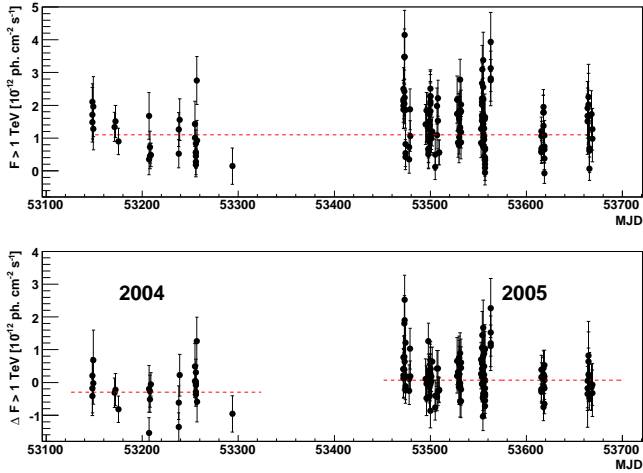


**Fig. 7. Top:** Integral flux ( $E > 1$  TeV) vs. time (MJD) for LS 5039 on a run-by-run basis. **Bottom:** After subtraction of the orbital period of 3.9063 days (this is achieved by subtraction of the Lomb-Scargle coefficients for the selected period). The average flux (dashed lines) for the post-subtracted light-curve is consistent with a steady source with a chance probability of  $4 \times 10^{-2}$ . In addition, the average flux levels determined exclusively for 2004 and 2005 data differ at a  $2\sigma$  level (statistical errors) but are consistent when factoring in systematic errors of  $\sim 10\%$  on a run-by-run basis.